

# Optical study on electronic structure of the locally non-centrosymmetric $\text{CeRh}_2\text{As}_2$

Shin-ichi Kimura,<sup>1,2,\*</sup> Jörg Sichelschmidt,<sup>3</sup> and Seunghyun Khim<sup>3</sup>

<sup>1</sup>*FBS and Department of Physics, Osaka University, Suita, Osaka 565-0871, Japan*

<sup>2</sup>*Institute for Molecular Science, Okazaki, Aichi 444-8585, Japan*

<sup>3</sup>*Max Planck Institute for Chemical Physics of Solids, 01187 Dresden, Germany*

(Dated: September 3, 2021)

The electronic structures of the heavy-fermion superconductor  $\text{CeRh}_2\text{As}_2$  with the local inversion symmetry breaking and the reference material  $\text{LaRh}_2\text{As}_2$  have been investigated by using experimental optical conductivity ( $\sigma_1(\omega)$ ) spectra and first-principal DFT calculations. In the low-temperature  $\sigma_1(\omega)$  spectra of  $\text{CeRh}_2\text{As}_2$ , a  $4f$ -conduction electron hybridization and heavy quasiparticles are clearly indicated by a mid-infrared peak and a narrow Drude peak. In  $\text{LaRh}_2\text{As}_2$ , these features are absent in the  $\sigma_1(\omega)$  spectrum, however, it can nicely be reproduced by DFT calculations. For both compounds, the combination between a local inversion symmetry breaking and a large spin-orbit (SO) interaction plays an important role for the electronic structure, however, the SO splitting bands could not be resolved in the  $\sigma_1(\omega)$  spectra due to the small SO splitting size.

## I. INTRODUCTION

Materials with non-centrosymmetric crystal structure and crystal surfaces with inversion symmetry breaking have recently attracted attention for novel physical properties combined with spin-orbit interaction (SOI) [1]. By using the SOI and the electric field gradient generated by the spatial symmetry breaking, a spin-polarized current originating from spin-polarized bands is generated and is regarded to be useful for spintronics applications. A breaking of local inversion symmetry also generates a toroidal current owing to the Dzyaloshinsky-Moriya interaction [2] and a Cooper pair with a helical spin structure, which produces a superconducting state with a high critical field [3]. Actually, an extremely high upper critical field  $H_{c2}$  as high as 5 T has been observed in the heavy-fermion superconductor  $\text{CePt}_3\text{Si}$  ( $T_c \sim 0.75$  K) having a globally non-centrosymmetric crystal structure [4].

$\text{CeRh}_2\text{As}_2$  has recently been discovered as a novel heavy-fermion superconductor ( $T_c = 0.26$  K) [6]. It crystallizes in the  $\text{CaBe}_2\text{Ge}_2$ -type structure ( $P4/nmm$ ), which lacks a local inversion symmetry of the Ce and one of the Rh and As sites while maintaining a global inversion center (see Fig. 1). Noteworthy, the majority of  $RM_2X_2$  ( $R = \text{rare earth}$ ,  $M = \text{transition metal}$ ,  $X = \text{Si, Ge}$ ) compounds including the first heavy-fermion superconductor  $\text{CeCu}_2\text{Si}_2$  [7] have a tetragonal  $\text{ThCr}_2\text{Si}_2$ -type crystal structure with inversion symmetry ( $I4/mmm$ ).

The fundamental physical properties of  $\text{CeRh}_2\text{As}_2$  including superconductivity have recently been reported [6]. The Kondo temperature ( $T_K$ ) and the electronic specific heat coefficient ( $\gamma$ ) have been evaluated as 20–40 K and  $\approx 1$  J/mol K<sup>2</sup> [6], respectively, which are similar to those of  $\text{CeCu}_2\text{Si}_2$  [8, 9]. The origin of the superconducting property of locally non-centrosymmetric heavy fermions including  $\text{CeRh}_2\text{As}_2$  has been investi-

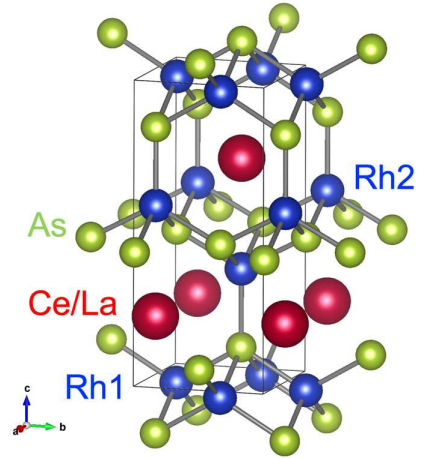


FIG. 1. Crystal structure of  $RRh_2As_2$  ( $R = \text{Ce, La}$ ) with the space group of  $P4/nmm$  depicted by using VESTA [5]. Rh 1 and Rh 2 are located at different sites and therefore have different effects on the electronic structure (see Figs. 4 and 6).

gated theoretically [10–16] and experimentally [17]. However, the electronic structure of the material, which is the most basic information for the discussion of the physical properties, has not been investigated experimentally so far, although the electronic structure using DFT calculations has been reported [13–15].

A locally non-centrosymmetric crystal structure can produce a local electric field to the electron orbitals. With a large SOI, the local electric field induces the band splitting such as the Rashba effect [18, 19], which can be directly observed by an angle-resolved photoelectron spectroscopy (ARPES) [20] and (magneto-optical) infrared spectroscopies [21–23]. ARPES studies on non-centrosymmetric heavy fermions have been performed on  $\text{CeIrSi}_3$  [24] and  $\text{UIr}$  [25]. However, so far, no studies of optical conductivity were reported for this type of materials.

\* kimura@fbs.osaka-u.ac.jp

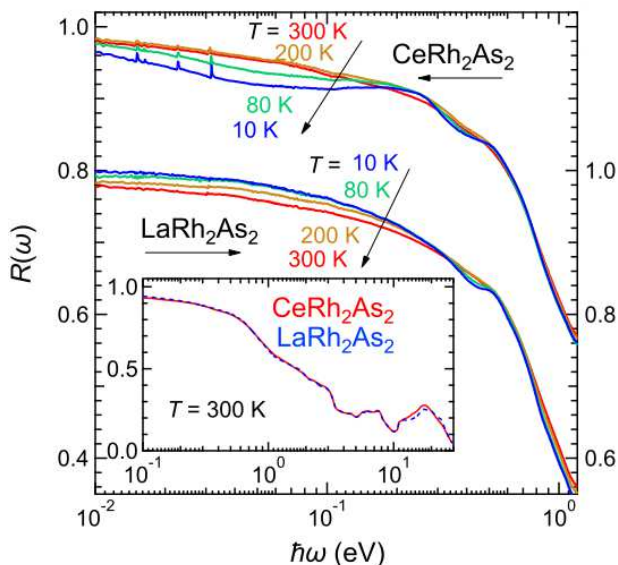


FIG. 2. Temperature-dependent reflectivity ( $R(\omega)$ ) spectra of the as-grown (001) surfaces of  $\text{CeRh}_2\text{As}_2$  and  $\text{LaRh}_2\text{As}_2$  in the photon energy  $\hbar\omega$  range of 0.01 – 1.2 eV. Fine structures of  $\text{CeRh}_2\text{As}_2$  at the photon energies  $\hbar\omega$  of about 15, 23, and 32 meV originate from TO phonons (not discussed here). (Inset) Wide-energy-range  $R(\omega)$  spectra of  $\text{CeRh}_2\text{As}_2$  and  $\text{LaRh}_2\text{As}_2$  in the  $\hbar\omega$  range of 0.1 – 30 eV at 300 K. Both spectra are almost identical suggesting the similar electronic structure at room temperature.

We investigated the fundamental electronic structure of the locally non-centrosymmetric heavy-fermion material  $\text{CeRh}_2\text{As}_2$  by measuring the optical conductivity ( $\sigma_1(\omega)$ ) spectra and comparing them with first-principal DFT calculations. As a reference material without 4*f* electrons, we also investigated  $\text{LaRh}_2\text{As}_2$  in order to discuss the electronic structure without the effect of the hybridization between conduction and 4*f* electrons (*c-f* hybridization). Firstly, the obtained  $\sigma_1(\omega)$  spectrum of  $\text{LaRh}_2\text{As}_2$  is compared with the DFT calculations for the fundamental electronic structure without 4*f* electrons. Next, the  $\sigma_1(\omega)$  spectrum of  $\text{CeRh}_2\text{As}_2$  is compared with the corresponding calculation results. Finally, the temperature-dependent  $\sigma_1(\omega)$  spectra of  $\text{CeRh}_2\text{As}_2$  is compared with other heavy fermion materials to discuss the evolution of the *c-f* hybridization.

## II. EXPERIMENT AND CALCULATION METHODS

Single-crystalline  $\text{CeRh}_2\text{As}_2$  and  $\text{LaRh}_2\text{As}_2$  samples were synthesized by the Bi-flux method [6]. The optical reflectivity  $R(\omega)$  measurements have been performed using the as-grown (001) plane. Near-normal-incident  $R(\omega)$  spectra were acquired in a wide photon-energy range of 8 meV – 30 eV to ensure accurate Kramers-

Kronig analysis (KKA) [26]. Infrared (IR) and terahertz (THz) measurements at the photon energy  $\hbar\omega$  regions of 8 meV–1.5 eV have been performed using conventional near-normal reflectivity measurement setups to obtain absolute  $R(\omega)$  at an accuracy of  $\pm 0.3\%$  with a feedback positioning system in the temperature range of 10–300 K [27]. To obtain the absolute  $R(\omega)$  values, the *in-situ* gold evaporation method was adopted. Obtained  $R(\omega)$  spectra of  $\text{CeRh}_2\text{As}_2$  and  $\text{LaRh}_2\text{As}_2$  are shown in Fig. 2. In the photon energy range of 1.5–30 eV, the  $R(\omega)$  spectrum was measured only at 300 K by using the synchrotron radiation setup at the beamline 3B of UVSOR-III Synchrotron [28], and connected to the spectra for  $\hbar\omega \leq 1.5$  eV for KKA. In order to obtain  $\sigma_1(\omega)$  via KKA of  $R(\omega)$ , the spectra were extrapolated below 8 meV with a Hagen-Rubens function [ $R(\omega) = 1 - \{2\omega/(\pi\sigma_{DC})\}^{1/2}$ ] due to the metallic  $R(\omega)$  spectra, and above 30 eV with a free-electron approximation  $R(\omega) \propto \omega^{-4}$  [29]. Here, the values of the direct current conductivity ( $\sigma_{DC}$ ) were adopted from the experimental values [6]. The extrapolations were confirmed not to severely affect to the  $\sigma_1(\omega)$  spectra at around 100 meV, which are the main part in this paper.

First-principal DFT calculations have been performed by using the WIEN2K code including SOI [30] to explain the experimentally obtained  $\sigma_1(\omega)$  spectra. Lattice parameters obtained from room-temperature x-ray diffraction measurements shown in Table I were adopted to the calculations. The obtained band structure of  $\text{CeRh}_2\text{As}_2$  was consistent with the recent report [13, 15].  $\sigma_1(\omega)$  spectra of the interband transitions have also been calculated by using the WIEN2K code. For the discussion of  $\text{LaRh}_2\text{As}_2$ , we also performed DFT calculations on the basis of a hypothetical  $\text{ThCr}_2\text{Si}_2$ -type crystal structure, assuming the same lattice constants as for the original  $\text{CaBe}_2\text{Ge}_2$ -type structure.

## III. RESULTS AND DISCUSSION

The measured  $R(\omega)$  spectra of  $\text{CeRh}_2\text{As}_2$  and  $\text{LaRh}_2\text{As}_2$ , shown in Fig. 2, at various temperatures, were used for KKA in order to obtain their  $\sigma_1(\omega)$  spectra as shown in Fig. 3. At 300 K,  $\sigma_1(\omega)$  of both materials monotonically increase with decreasing  $\hbar\omega$  suggesting a typical metallic character. The spectrum of  $\text{CeRh}_2\text{As}_2$  at 300 K is very similar to that of  $\text{LaRh}_2\text{As}_2$ , as demonstrated by almost identical  $R(\omega)$  spectra in the inset of Fig. 2. This suggests fully localized Ce 4*f* states at 300 K. With decreasing temperature, the spectra strongly change and new features emerge: A double-peak structure (“mid-IR peak”) appears at 0.12 and 0.4 eV in  $\text{CeRh}_2\text{As}_2$ , whereas in  $\text{LaRh}_2\text{As}_2$ , a weak single peak becomes visible at 0.45 eV. The mid-IR peak is usually observed in many Ce compounds and suggests the emergence of the *c-f* hybridization [31]. The peak appearing in  $\text{LaRh}_2\text{As}_2$  does not obviously originate from the *c-f* hybridization, but can be explained by the electronic structure of  $\text{LaRh}_2\text{As}_2$ .

TABLE I. Lattice parameters of  $\text{CeRh}_2\text{As}_2$  and  $\text{LaRh}_2\text{As}_2$  used for the DFT calculations. The parameters were obtained by x-ray diffraction methods.

Sample	$\text{CeRh}_2\text{As}_2$			$\text{LaRh}_2\text{As}_2$		
Crystal structure	CaBe <sub>2</sub> Ge <sub>2</sub> -type					
Space group	$P_4/nmm$ (No. 129)					
Lattice constant						
a (Å), b (Å), c (Å)	4.283(1)	4.283(1)	9.865(2)	4.3137(2)	4.3137(2)	9.8803(4)
Position	X	Y	Z	X	Y	Z
Ce, La	0.25	0.25	0.254686(3)	0.25	0.25	0.2543(2)
Rh 1	0.75	0.25	0	0.75	0.25	0
Rh 2	0.25	0.25	0.617418(4)	0.25	0.25	0.6159(2)
As 1	0.75	0.25	0.5	0.75	0.25	0.5
As 2	0.25	0.25	0.864075(7)	0.25	0.25	0.871(9)

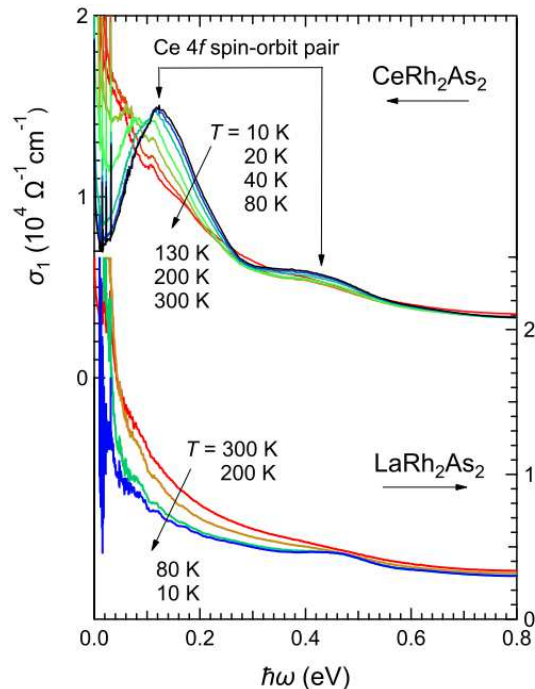


FIG. 3. Temperature-dependent optical conductivity ( $\sigma_1(\omega)$ ) spectra of  $\text{CeRh}_2\text{As}_2$  and  $\text{LaRh}_2\text{As}_2$ .

#### A. Electronic structure of $\text{LaRh}_2\text{As}_2$

Figure 4 shows the band calculation results of  $\text{LaRh}_2\text{As}_2$  near the Fermi energy ( $E_F$ ) with and without SOI. The main effect of including the SOI appears as a spin-orbit (SO) splitting near  $E_F$  along the  $M-X$  and  $A-R$  lines (see the red encircled regions in Fig. 4). The bands mainly originate from the  $4d$  states of Rh 1 as shown in the partial density of states depicted in Fig. 4. The SO splitting is much smaller than that of  $\text{LaPt}_3\text{Si}$  [32] and  $\text{BiTeI}$  [23]. The different SO splitting size probably originate from the different orbital moments ( $4d$  for Rh,  $5d$  for Pt, and  $6p$  for Bi), locally/globally non-centrosymmetric crystal structure,

and/or the different dimensionality, three-dimensional  $\text{LaRh}_2\text{As}_2$  and  $\text{LaPt}_3\text{Si}$ , and two-dimensional  $\text{BiTeBr}$ .

Figure 5 shows the experimental  $\sigma_1(\omega)$  spectrum of  $\text{LaRh}_2\text{As}_2$  at  $T = 10$  K together with spectra obtained from the DFT calculation results (Fig. 4) either with SOI (red solid line) or without SOI (blue solid line). The free charge carrier response (Drude peak, grey solid line) evaluated from  $\sigma_{DC}$  of  $\text{LaRh}_2\text{As}_2$  is also shown. The experimental  $\sigma_1(\omega)$  spectrum (denoted by “Experiment” in Fig. 5) is much larger than the expected Drude curve suggesting the existence of other components due to interband transitions overlapping on the Drude curve. These interband transitions are indicated by the thick solid line (denoted by “Experiment - Drude” in Fig. 5), which was derived by subtraction of the Drude curve from the  $\sigma_1(\omega)$  spectrum. The interband transition spectrum has a broad peak at around  $\sim 0.1$  eV and a sharp peak at  $\sim 0.5$  eV.

Both calculated  $\sigma_1(\omega)$  spectra with and without SOI are almost identical suggesting a weak effect of the SOI on  $\sigma_1(\omega)$ . This is consistent with the small SOI intensity of  $\text{LaRh}_2\text{As}_2$ . The two significant peaks at  $\hbar\omega \sim 0.2$  eV and  $0.45$  eV can be attributed to the experimentally observed peaks at  $\sim 0.1$  eV and  $\sim 0.5$  eV. They both originate from the bands near the  $\Gamma-M$  and  $Z-A$  lines in the Brillouin zone (see Fig. 4). The background intensity of the calculated spectra is consistent with that of the experimental spectrum. Therefore, the experimental  $\sigma_1(\omega)$  spectrum can be explained well by the DFT calculations.

In order to investigate the effect of the crystal structure, Fig. 5 also shows a  $\sigma_1(\omega)$  spectrum calculated by using the centrosymmetric  $\text{ThCr}_2\text{Si}_2$ -type crystal structure ( $I4/mmm$ ) while keeping the lattice parameters as in the  $\text{CaBe}_2\text{Ge}_2$ -type structure. The large peak at  $\sim 0.5$  eV does not appear and the background spectral intensity is much lower than that of the experimental spectrum. This suggests that both the  $0.5$  eV peak and the high background intensity are characteristic properties of  $\text{LaRh}_2\text{As}_2$  and the locally non-centrosymmetric  $\text{CaBe}_2\text{Ge}_2$ -type crystal structure.

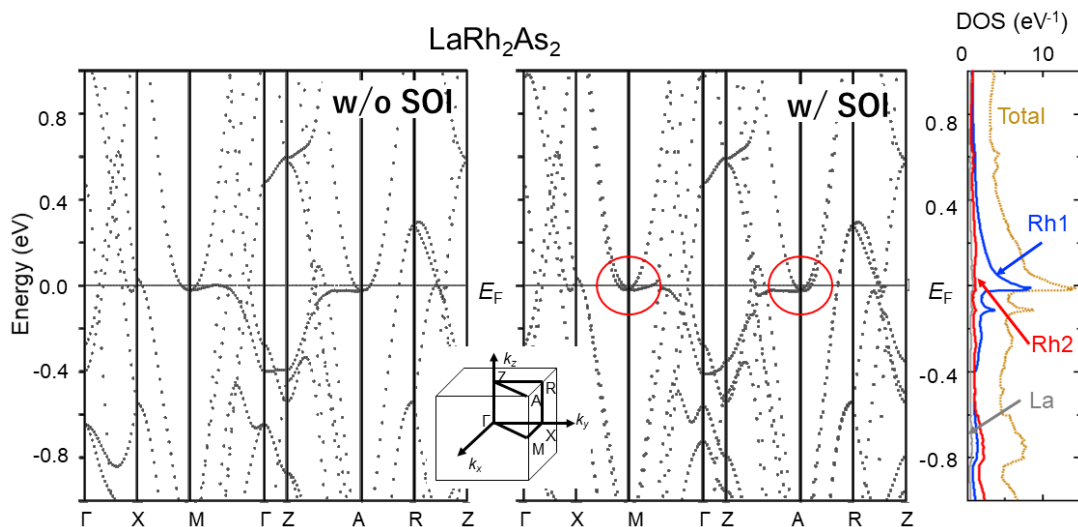


FIG. 4. Calculated band structure of  $\text{LaRh}_2\text{As}_2$  without (left) SOI and with (center) SOI. Spin-orbit splitted bands are red encircled. Inset depicts symmetry points in the Brillouin zone. (Right) Total density of states and partial density of states of La, Rh 1 and Rh 2 (see Fig. 1) with SOI.

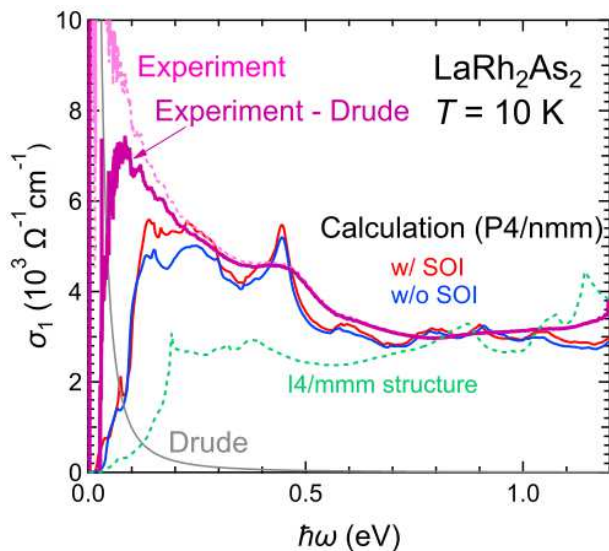


FIG. 5. Optical conductivity ( $\sigma_1(\omega)$ ) spectrum of  $\text{LaRh}_2\text{As}_2$  at  $T = 10$  K (Experiment, dotted line). Thick line denotes the interband transition part obtained after subtracting the Drude part (grey line) from the  $\sigma_1(\omega)$  spectrum. Calculated  $\sigma_1(\omega)$  spectra with and without SOI are shown by red and blue lines, respectively. The calculated spectrum of a centrosymmetric  $\text{ThCr}_2\text{Si}_2$ -type crystal structure ( $I4/mmm$ ) is also plotted for comparison (dashed green line).

### B. Electronic structure of $\text{CeRh}_2\text{As}_2$

Figure 6 shows the calculated band structures of  $\text{CeRh}_2\text{As}_2$  with and without SOI. An important effect of the SOI is a splitting of the Ce  $4f$  bands from almost

flat bands at  $\sim 0.3$  eV into two parts, namely  $4f_{5/2}$  bands at  $\sim 0.2$  eV and  $4f_{7/2}$  bands at  $\sim 0.5$  eV. The splitting energy is roughly  $0.25 - 0.3$  eV, which is a characteristic value for various Ce-based compounds as observed in  $\sigma_1(\omega)$  spectra [31, 33] and photoelectron spectra [8, 34].

As in  $\text{LaRh}_2\text{As}_2$ , the SO split bands appear near  $E_F$  along the  $M-X$  and  $A-R$  lines. The size of SO splitting is larger than that of  $\text{LaRh}_2\text{As}_2$ . Since the bands originate from the hybridization between the Rh 1  $4d$  and Ce  $4f$  bands (see the partial densities of states of Ce and Rh 1 in the right figure of Fig. 6), the  $4f$  state is considered to be relevant for the SO splitting. Moreover, as flat bands are claimed to be important for the superconductivity [13], the SO splitting may play an important role for the exotic superconductivity in  $\text{CeRh}_2\text{As}_2$ .

Figure 7 shows the experimentally obtained  $\sigma_1(\omega)$  spectrum at  $T = 10$  K together with the calculated  $\sigma_1(\omega)$  spectra with and without SOI. In comparison with the  $\sigma_1(\omega)$  spectra of  $\text{LaRh}_2\text{As}_2$ , the calculated spectra cannot reproduce the experimental spectrum well. The main reason is that the mid-IR peak below  $\hbar\omega \sim 0.6$  eV does not appear in the calculation. The experimental mid-IR peak can be attributed to the SO splitting of the Ce  $4f$  states [35], which appears in the unoccupied density of states above  $E_F$  as shown in the lower frame of Fig. 7. However, the corresponding mid-IR peak structure does not clearly appear in the  $\sigma_1(\omega)$  calculation shown in the upper frame of Fig. 7. The inconsistency suggests that the calculated  $c-f$  hybridization intensity in the DFT calculations is much smaller than the experimental value because the Kondo interaction between conduction and localized  $4f$  electrons is not included in the calculation.

According to the band calculation in Fig. 6, the signature of the SO splitting along the  $\Gamma-M$  line may appear



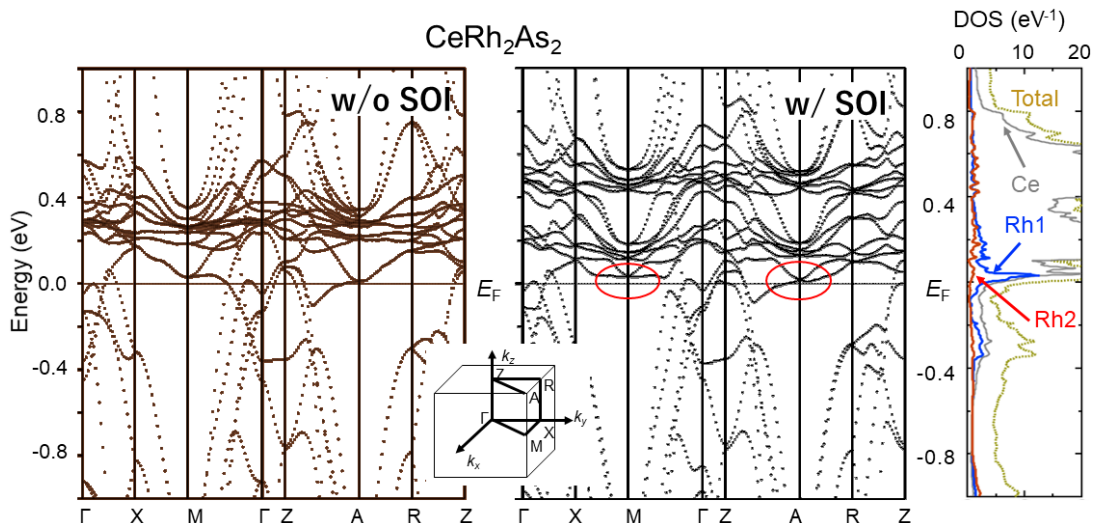


FIG. 6. Calculated band structure of  $\text{CeRh}_2\text{As}_2$  without (left) SOI and with (center) SOI. Spin-orbit splitted bands are red encircled. Inset depicts symmetry points in the Brillouin zone. (Right) Total density of states and partial density of states of Ce, Rh 1 and Rh 2 (see Fig. 1) with SOI.

at  $\hbar\omega \leq 0.1$  eV. In this energy region, there are three phonon peaks at  $\hbar\omega = 15.2, 22.8,$  and  $31.7$  meV (see Fig. 2), but no other significant structures except for the Drude peak. Therefore, we conclude that, in the  $\sigma_1(\omega)$  spectra, there are no visible signatures for a SO splitting expected in the band structure.

### C. $c$ - $f$ hybridization of $\text{CeRh}_2\text{As}_2$

The  $c$ - $f$  hybridization in  $\text{CeRh}_2\text{As}_2$  can be characterized by using the temperature dependence of the mid-IR peak. Figure 8 shows the temperature dependencies of the center of gravity  $[\Delta\langle\omega\rangle = [\langle\omega(T)\rangle - \langle\omega(300\text{ K})\rangle] / \langle\omega(300\text{ K})\rangle]$ , where  $\langle\omega(T)\rangle = \int_{\omega_1}^{\omega_2} \omega \sigma_1(\omega) d\omega / \int_{\omega_1}^{\omega_2} \sigma_1(\omega) d\omega$ , and the spectral weight transfer  $[\Delta SW = \int_{\omega_1}^{\omega_2} [|\sigma_1(\omega, T) - \sigma_1(\omega, 300\text{ K})| / \sigma_1(\omega, 300\text{ K})] d\omega]$  of the mid-IR peak of  $\text{CeRh}_2\text{As}_2$  relative to those at  $T = 300$  K. The integration range was set as  $\omega_1 = 0$  eV  $\leq \omega \leq \omega_2 = 0.8$  eV, where the spectral change in the lower energy region is almost recovered. In the figure, the evaluated  $\Delta\langle\omega\rangle$  and  $\Delta SW$  of two heavy-fermion compounds  $\text{CeCu}_2\text{Si}_2$  ( $T_K \sim 10$  K) [36] and  $\text{CeNi}_2\text{Ge}_2$  ( $T_K \sim$  several K) [33] are also plotted for comparison. The temperature dependencies of  $\Delta\langle\omega\rangle$  and  $\Delta SW$  correspond to the evolution of the  $c$ - $f$  hybridization with temperature [31], i.e., an increasing itinerancy corresponds to increasing values of  $\Delta\langle\omega\rangle$  and  $\Delta SW$  whereas constant values suggest a localization of the  $4f$  state.

In  $\text{CeRh}_2\text{As}_2$ ,  $\Delta\langle\omega\rangle$  is constant near 300 K and increases toward low temperatures below  $\sim 150$  K, suggesting a rapid development of the  $c$ - $f$  hybridization below the temperature. This is consistent with the  $c$ - $f$  hy-

bridization intensity being almost negligible at 300 K, which is demonstrated by almost identical  $R(\omega)$  spectra of  $\text{CeRh}_2\text{As}_2$  and  $\text{LaRh}_2\text{As}_2$  at 300 K (see inset of Fig. 2).

The  $\Delta SW$  values monotonically increase with decreasing temperature below 300 K. As was shown previously [31], an increase from 300 K to  $\sim 100$  K originates from electron-phonon interactions, and the  $c$ - $f$  hybridization effect appears below the temperature of  $\sim 100$  K. In  $\text{CeRh}_2\text{As}_2$ , the  $\Delta SW$  increases at low temperatures, which is consistent with  $\Delta\langle\omega\rangle$ . The values of  $\Delta\langle\omega\rangle$  and  $\Delta SW$  of  $\text{CeRh}_2\text{As}_2$  at the lowest accessible temperature are located in between those of  $\text{CeCu}_2\text{Si}_2$  and  $\text{CeNi}_2\text{Ge}_2$  suggesting an intermediate  $c$ - $f$  hybridization intensity  $\tilde{V}$ , which is included in the Kondo temperature expression

$$T_K \propto \exp[-\tilde{V}^{-2} D_c(E_F)^{-1}],$$

where  $D_c(E_F)$  is the density of states of the conduction band at  $E_F$  [37]. Hence, compared to  $\text{CeCu}_2\text{Si}_2$ , the higher  $T_K \sim 20$ – $40$  K and smaller  $\tilde{V}$  of  $\text{CeRh}_2\text{As}_2$  should be related to a larger  $D_c(E_F)$ . Indeed, such conclusion is consistent with the  $\sigma_1(\omega)$  spectral intensity of  $\text{LaRh}_2\text{As}_2$  for  $\hbar\omega \leq 0.8$  eV, which reflects the density of states near the  $E_F$ . In this region,  $\sigma_1(\omega)$  is enhanced compared to the calculated one using the  $\text{ThCr}_2\text{Si}_2$ -type structure as shown in Fig. 5, which is also due to a flat Rh  $4d$  band near the  $E_F$  as shown in Fig. 4. Therefore, the locally non-centrosymmetric  $\text{CaBe}_2\text{Ge}_2$ -type crystal structure of  $\text{CeRh}_2\text{As}_2$  supports a higher  $T_K$  than the  $\text{ThCr}_2\text{Si}_2$ -type structure of  $\text{CeCu}_2\text{Si}_2$ .

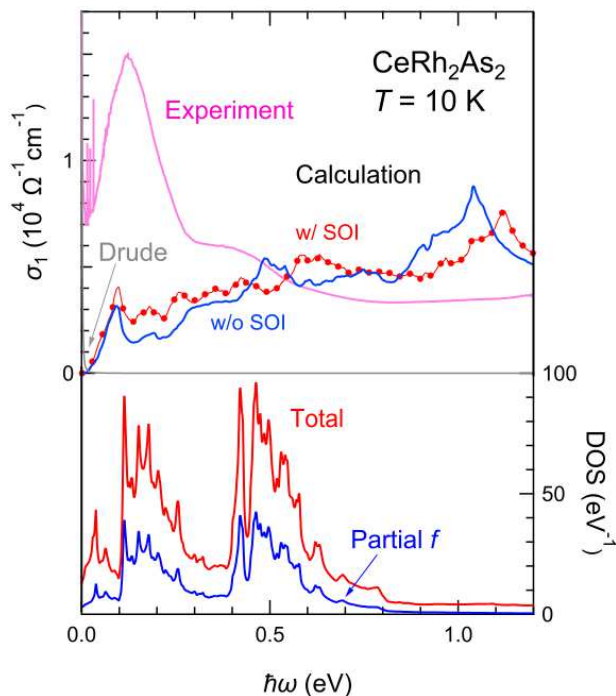


FIG. 7. Optical conductivity ( $\sigma_1(\omega)$ ) spectrum of  $\text{CeRh}_2\text{As}_2$  at 10 K (Experiment, magenta solid line). The Drude curve expected by the experimental electrical resistivity is shown by a gray solid line, and calculated  $\sigma_1(\omega)$  spectra with and without SOI are shown by a red marked line and a blue solid line, respectively. The total and partial  $f$  density of states above  $E_F$  are also plotted in the lower figure for the comparison with the  $\sigma_1(\omega)$  spectrum. The  $E_F$  of the density of states is set to  $\hbar\omega = 0$  eV of  $\sigma_1(\omega)$  spectra. The peaks at about 0.2 and 0.5 eV originate from the unoccupied Ce  $4f_{5/2}$  and  $4f_{7/2}$  states.

#### IV. CONCLUSION

To summarize, optical conductivity  $\sigma_1(\omega)$  spectra of a locally non-centrosymmetric heavy fermion superconductor  $\text{CeRh}_2\text{As}_2$  and  $\text{LaRh}_2\text{As}_2$  as a fermion material without  $4f$  electrons were measured and compared with the corresponding DFT calculations. The experimentally obtained  $\sigma_1(\omega)$  spectrum of  $\text{LaRh}_2\text{As}_2$  can be explained well by the DFT calculations. Besides, the experimental

$\sigma_1(\omega)$  spectrum of  $\text{CeRh}_2\text{As}_2$  at low temperatures has a stronger  $c$ - $f$  hybridization intensity than the DFT calculation because the Kondo interaction is effective at low temperatures, which is also seen in the temperature dependence of the  $\sigma_1(\omega)$  spectrum. The evidence of the SO splitting due to the locally non-centrosymmetric crystal structure, unfortunately, could not be observed in the  $\sigma_1(\omega)$  spectra because of the SO splitting being too small for resolvable spectral features.

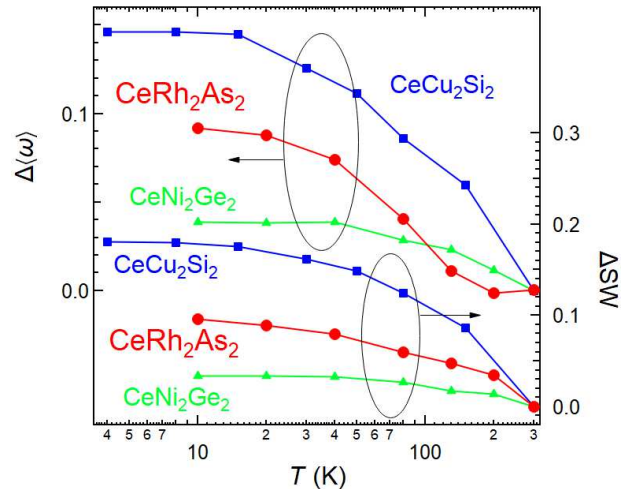


FIG. 8. Relative temperature dependence of the change of the center of gravity ( $\Delta\langle\omega\rangle$ , left axis) and the spectral weight ( $\Delta SW$ , right axis) of  $\text{CeRh}_2\text{As}_2$  and reference materials,  $\text{CeCu}_2\text{Si}_2$  and  $\text{CeNi}_2\text{Ge}_2$  [31]. These values were normalized to their room-temperature values.

#### ACKNOWLEDGMENTS

We would like to thank Profs. Noriaki Kimura, Takahiro Ito, Hiroshi Watanabe, and Yoshiyuki Ohtsubo for their fruitful discussion and UVSOR Synchrotron staff members for their support during synchrotron radiation experiments. Part of this work was performed under the Use-of-UVSOR Synchrotron Facility Program (Proposals No. 20-735) of the Institute for Molecular Science, National Institutes of Natural Sciences. This work was partly supported by JSPS KAKENHI (Grant No. 20H04453).

- 
- [1] Y. P. Feng, L. Shen, M. Yang, A. Wang, M. Zeng, Q. Wu, S. Chintalapati, and C.-R. Chang, Wiley Interdiscip. Rev. Comput. Mol. Sci. **7**, e1313 (2017).  
 [2] J. M. Crabtree and A. Soncini, Phys. Rev. B **98**, 094417 (2018).  
 [3] P. A. Frigeri, D. F. Agterberg, A. Koga, and M. Sigrist, Phys. Rev. Lett. **92**, 097001 (2004), arXiv:0311354 [cond-mat].  
 [4] E. Bauer, G. Hilscher, H. Michor, C. Paul, E. W. Scheidt, A. Griбанov, Y. Seropegin, H. Noël, M. Sigrist, and P. Rogl, Phys. Rev. Lett. **92**, 027003 (2004).  
 [5] K. Momma and F. Izumi, J. Appl. Crystallogr. **44**, 1272 (2011).  
 [6] S. Khim, J. F. Landaeta, J. Banda, N. Bannor, M. Brando, P. M. R. Brydon, D. Hafner, R. Kuchler, R. Cardoso-Gil, U. Stockert, A. P. Mackenzie, D. F. Agterberg, C. Geibel, and E. Hassinger, Science (80-. ). **373**, 1012 (2021), arXiv:2101.09522.  
 [7] F. Steglich, J. Aarts, C. D. Bredl, W. Lieke, D. Meschede, W. Franz, and H. Schäfer,

- Phys. Rev. Lett. **43**, 1892 (1979).
- [8] F. Reinert, D. Ehm, S. Schmidt, G. Nicolay, S. Hüfner, J. Kroha, O. Trovarelli, and C. Geibel, Phys. Rev. Lett. **87**, 106401 (2001).
- [9] S. Kittaka, Y. Aoki, Y. Shimura, T. Sakakibara, S. Seiro, C. Geibel, F. Steglich, H. Ikeda, and K. Machida, Phys. Rev. Lett. **112**, 067002 (2014), arXiv:1307.3499.
- [10] T. Yoshida, M. Sigrist, and Y. Yanase, Phys. Rev. Lett. **115**, 027001 (2015), arXiv:1507.06388.
- [11] E. G. Schertenleib, M. H. Fischer, and M. Sigrist, Phys. Rev. Res. **3**, 023179 (2021), arXiv:2101.08821.
- [12] A. Skurativska, M. Sigrist, and M. H. Fischer, Phys. Rev. Res. **3**, 033133 (2021), arXiv:2103.06282.
- [13] K. Nogaki, A. Daido, J. Ishizuka, and Y. Yanase, (2021), arXiv:2103.08088.
- [14] A. Ptok, K. J. Kapcia, P. T. Jochym, J. Łażewski, A. M. Oleś, and P. Piekarczyk, Phys. Rev. B **104**, L041109 (2021), arXiv:2102.02735.
- [15] D. C. Cavanagh, T. Shishidou, M. Weinert, P. M. R. Brydon, and D. F. Agterberg, , 1 (2021), arXiv:2106.02698.
- [16] D. Möckli and A. Ramires, Phys. Rev. Res. **3**, 023204 (2021), arXiv:2102.09425.
- [17] D. Hafner, P. Khanenko, E. O. Eljaouhari, R. Küchler, J. Banda, N. Bannor, T. Lühmann, J. F. Landaeta, S. Mishra, I. Sheikin, E. Hassinger, S. Khim, C. Geibel, G. Zwicknagl, and M. Brando, (2021), arXiv:2108.06267.
- [18] E. I. Rashba and V. I. Sheka, Dtsch. Phys. Gesellschaft **2**, 162 (1959).
- [19] G. Bihlmayer, O. Rader, and R. Winkler, New J. Phys. **17**, 050202 (2015).
- [20] K. Ishizaka, M. S. Bahrany, H. Murakawa, M. Sakano, T. Shimojima, T. Sonobe, K. Koizumi, S. Shin, H. Miyahara, A. Kimura, K. Miyamoto, T. Okuda, H. Namatame, M. Taniguchi, R. Arita, N. Nagaosa, K. Kobayashi, Y. Murakami, R. Kumai, Y. Kaneko, Y. Onose, and Y. Tokura, Nat. Mater. **10**, 521 (2011).
- [21] L. Demkó, G. A. H. Schober, V. Kocsis, M. S. Bahrany, H. Murakawa, J. S. Lee, I. Kézsmárki, R. Arita, N. Nagaosa, and Y. Tokura, Phys. Rev. Lett. **109**, 167401 (2012).
- [22] C. Martin, E. D. Mun, H. Berger, V. S. Zapf, and D. B. Tanner, Phys. Rev. B **87**, 041104 (2013).
- [23] C. Martin, A. V. Suslov, S. Buvaev, A. F. Hebard, P. Bugnon, H. Berger, A. Magrez, and D. B. Tanner, EPL (Europhysics Lett. **116**, 57003 (2016).
- [24] T. Ohkochi, T. Toshimitsu, H. Yamagami, S.-i. Fujimori, A. Yasui, Y. Takeda, T. Okane, Y. Saitoh, A. Fujimori, Y. Miyauchi, Y. Okuda, R. Settai, and Y. Ōnuki, J. Phys. Soc. Japan **78**, 084802 (2009).
- [25] H. Yamagami, T. Ohkochi, S. I. Fujimori, T. Toshimitsu, A. Yasui, T. Okane, Y. Saitoh, A. Fujimori, Y. Haga, E. Yamamoto, S. Ikeda, and Y. Onuki, J. Phys. Conf. Ser. **200**, 8 (2010).
- [26] S.-i. Kimura and H. Okamura, J. Phys. Soc. Japan **82**, 021004 (2013), arXiv:1210.5310.
- [27] S.-i. Kimura, Jasco Rep. **50**, 6 (2008).
- [28] K. Fukui, R.-i. Ikematsu, Y. Imoto, M. Kitaura, K. Nakagawa, T. Ejima, E. Nakamura, M. Sakai, M. Hasumoto, and S.-i. Kimura, J. Synchrotron Radiat. **21**, 452 (2014).
- [29] M. Dressel and G. Grüner, Electrodyn. Solids (Cambridge University Press, 2002).
- [30] P. Blaha, K. Schwarz, P. Sorantin, and S. Trickey, Comput. Phys. Commun. **59**, 399 (1990).
- [31] S.-i. Kimura, Y. S. Kwon, C. Krellner, and J. Sichelschmidt, Electron. Struct. **3**, 024007 (2021), arXiv:2101.09696.
- [32] H. Uzunok, H. Tütüncü, G. Srivastava, and A. Başoğlu, Intermetallics **86**, 1 (2017).
- [33] S.-i. Kimura, Y. S. Kwon, Y. Matsumoto, H. Aoki, and O. Sakai, J. Phys. Soc. Japan **85**, 083702 (2016), arXiv:1605.04981.
- [34] H. Im, T. Ito, S. Kimura, J. Hong, and Y. Kwon, Phys. B Condens. Matter **378-380**, 825 (2006).
- [35] S.-i. Kimura, T. Iizuka, and Y.-s. Kwon, J. Phys. Soc. Japan **78**, 013710 (2009), arXiv:0811.2869.
- [36] J. Sichelschmidt, A. Herzog, H. S. Jeevan, C. Geibel, F. Steglich, T. Iizuka, and S. Kimura, J. Phys. Condens. Matter **25**, 1 (2013), arXiv:1301.2896.
- [37] A. C. Hewson, The Kondo Problem to Heavy Fermions (Cambridge University Press, Cambridge, 1993).